

Getting Stuck!

Using Monosignatures to Test Highly Ionizing Particles

Christoph Englert¹ and Joerg Jaeckel²

¹*SUPA, School of Physics and Astronomy, University of Glasgow,
Glasgow G12 8QQ, United Kingdom*

²*Institut für Theoretische Physik, Universität Heidelberg,
Philosophenweg 16, 69120 Heidelberg, Germany*

Abstract

In this paper we argue that monojet and monophoton searches can be a sensitive test of very highly ionizing particles such as particles with charges $\gtrsim 150e$ and more generally particles that do not reach the outer parts of the detector. 8 TeV monojet data from the CMS experiment excludes such objects with masses in the range $\lesssim 650$ GeV and charges $\gtrsim 100e$. This nicely complements searches for highly ionizing objects at ALICE, ATLAS, CMS and LHCb. Expected improvements in these channels will extend the sensitivity range to $m \lesssim 750$ GeV. This search strategy can directly be generalized to other particles that strongly interact with the detector material, such as e.g. magnetic monopoles.

1 Introduction

Monojet and monophoton searches are a popular tool to search for particles interacting so weakly with the detector that they do not leave an observable trace. In particular they have become one of the main avenues to search for dark matter particles at colliders, see e.g. [1–6].

At the very opposite extreme one can imagine particles that interact so strongly with matter that they are stopped before they reach essential parts of the detector, such as the calorimeters, which is required for triggering and eventual detection. In some cases they may be stopped even before they leave the beam pipe, such that there is no chance that they can be directly detected with the usual multi-purpose detectors. Examples of candidate particles interacting very strongly with matter are particles with high electric charges or magnetic monopoles (perhaps even with multiple magnetic charges) [7, 8]. This shortcoming of the Large Hadron Collider’s multi-purpose experiments is part of the motivation of the MoEDAL experiment [9], which has published first results in Ref. [10].

The main goal of this note is to point out that monojet and monophoton searches at the multi-purpose detectors are also a powerful tool to search for such super-strongly interacting particles, which nicely complement and extend the sensitivity reach of these LHC experiments. The idea is quite straightforward: if the produced particles are so strongly interacting that they are stopped before they leave a recognizable trace in the detector they are just as “invisible” as particles that are very weakly interacting. This sets the limitation in general searches for highly ionizing particles (HIPs) in Drell-Yan-like production [11], Fig. 1. However, if these objects have a large mass in the 100 GeV range, this mass scale will induce a shower signature to the full hadronic final state via coherent initial and/or final state radiation. Since this is a purely kinematics-driven phenomenon based on QCD factorisation, at least the appearance of initial state radiation should not be dependent on the particular production mechanism of the HIP and will occur even if production is intrinsically non-perturbative, which can be expected for extended objects such as monopoles. This way, even if we have no triggerable signature (identically to very weakly interacting particles), there is a potential signature from the recoil of the HIP against additional Standard Model emission, leading to monophoton, mono- Z and monojet signatures.

We will demonstrate in this paper that highly charged particles can be constrained at the LHC employing “standard” dark matter searches. This can be generalised to searches for other highly ionising particles such as magnetic monopoles. We will argue that monojet and monophoton searches are highly complementary to the on-going search efforts at the LHC, but also complementary to MoEDAL, leading to large increase of sensitivity to these scenarios.

This brief note is structured as follows. In the following two sections we start with the concrete example of particles with large electric charges. We recall how they are stopped in Sec. 2 and what this implies for searching them with monojet and monophoton searches. The actual limits are presented in Sec. 3. To put this into perspective we discuss some potential issues with highly charged particles and their description in Sec. 4. In Sec. 5 we then discuss more general aspects applicable to wider classes of particles. We end with concluding words in Sec. 6.

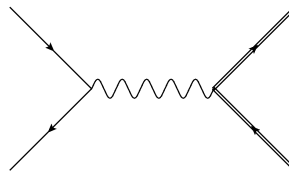


Figure 1: Drell-Yan production of a highly charged particle (indicated by a double line).

2 Producing and stopping particles with high electric charges

To demonstrate the general idea of searching for very strongly interacting particles with monojet and monophoton searches we consider the concrete example of highly charged particles, more concretely highly charged fermions. But even at this point we would like to stress that the approach more generally applies to particles that have a significant chance of being stopped before they reach an essential part of the detector.

2.1 Productions with monojet and monophoton

The simplest production mechanism of highly charged particles is Drell-Yan (cf. Fig. 1), which is typically employed to provide estimates for collider searches (see [9, 11–23]). However, if the particles are stopped they alone will not produce a detectable signal. We will therefore consider monojet and monophoton processes, examples of which are depicted Figs. 2 and 3.

2.2 Stopping highly charged particles

An essential ingredient for our search strategy is that the produced highly charged particles are stopped early enough. Let us now estimate when and how this happens.

To do so we follow [11] and use the Bethe-Bloch formula for the energy loss of charged particles with velocity β , gamma-factor γ and charge z (in units of e) in materials,

$$-\frac{dE}{dx} = K \frac{Z}{A} \frac{z^2}{\beta^2} \left[\log \left(\frac{2m_e \beta^2 \gamma^2}{I} \right) - \beta^2 \right]. \quad (2.1)$$

Here x is the amount of material per area traversed, effectively,

$$x = \rho \ell \quad (2.2)$$

where ℓ is the distance travelled in the medium of density ρ .

In the Bethe-Bloch equation we also have the constant,

$$K = 0.307 \text{ MeV g}^{-1} \text{ cm}^2, \quad (2.3)$$

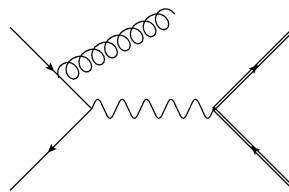


Figure 2: Representative Feynman diagram of Drell-Yan production of a highly charged particle (double line) in association with the production of a single gluon from initial state radiation, eventually giving rise to a monojet signature.

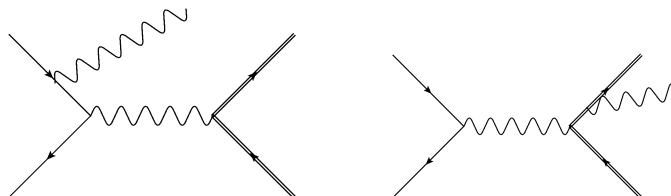


Figure 3: Representative diagrams for Drell-Yan production leading to a monophoton signature. The photon can be radiated off the initial but also the final state particle, see text.

and we need to specify the material properties. Z and A are the nuclear charge and nucleon number of the atoms of the medium. Finally I is the mean excitation energy in the medium, which is documented in the PDG review [24] for the two relevant materials we consider,

$$\begin{aligned} {}^9\text{Be} &: A = 9, \quad Z = 4, \quad I = 63.7 \text{ eV} && \text{beam pipe}, \\ {}^{28}\text{Si} &: A = 28, \quad Z = 14, \quad I = 137 \text{ eV} && \text{inner tracker}. \end{aligned} \quad (2.4)$$

To determine whether the particle gets stuck we need to integrate the Bethe-Bloch equation up to the point where the highly charged particle has lost all its kinetic energy, i.e. $\gamma = 1$. Using $E = \gamma m$ one can easily scale out the mass and charge dependence from the Bethe-Bloch equation. The distance travelled in a given (fixed) material is then given by,

$$x_{\text{stop}} = \left(\frac{100}{z} \right)^2 \left(\frac{m}{1 \text{ TeV}} \right) f_{\text{mat}}(\gamma) \frac{g}{\text{cm}^2}. \quad (2.5)$$

The function f_{mat} only depends on the material and the initial gamma-factor of the highly charged particle. Integrating the Bethe-Bloch equation for different values of γ we find the following fitting functions,

$$f_{\text{Be}}(\gamma) = \begin{cases} 0.25 & \text{for } \gamma \lesssim 1.05 \\ 29.7766 - 69.2787\gamma + 39.2006\gamma^2 & \text{for } 1.05 \lesssim \gamma \lesssim 1.5 \\ -72.5575 + 57.5741\gamma - 0.159835\gamma^2 & \text{for } 1.5 \lesssim \gamma \lesssim 50 \end{cases} \quad (2.6)$$

and

$$f_{\text{Si}}(\gamma) = \begin{cases} 0.26 & \text{for } \gamma \lesssim 1.05 \\ 28.6498 - 67.4852\gamma + 38.5221\gamma^2 & \text{for } 1.05 \lesssim \gamma \lesssim 1.5 \\ -69.0793 + 55.7173\gamma - 0.167437\gamma^2 & \text{for } 1.5 \lesssim \gamma \lesssim 50 \end{cases}. \quad (2.7)$$

We will use these functions directly in our Monte Carlo simulation, they are accurate within about 15%.

We can now determine whether a particle of given mass, charge, momentum and direction will be stopped in the beam pipe or in the inner tracker. As in [11] we use a “thickness” of the beam pipe and inner tracker of

$$\begin{aligned} \text{beam pipe :} \quad d_{\text{bp}} &= 0.148 \frac{\text{g}}{\text{cm}^2} \quad (\text{Beryllium}) \\ \text{inner tracker :} \quad d_{\text{it}} &= 9.6 \frac{\text{g}}{\text{cm}^2} \quad (\text{Silicon}). \end{aligned} \quad (2.8)$$

For a given energy, mass and pseudo-rapidity the minimal charge required to stop the particle is then given by

$$Q_{\text{min}}(E, \eta) = 100 \sqrt{f \left(\frac{E}{m} + 1 \right) \left(\frac{m}{\text{TeV}} \right) \frac{1}{x(\eta)}} \quad (2.9)$$

with

$$x(\eta) = \frac{d}{\sin(\theta)} = \frac{d}{\sin(2 \arctan[\exp[-\eta]])}, \quad (2.10)$$

where d is either d_{bp} for the beam pipe or d_{it} for the inner tracker. The angular/pseudo-rapidity dependence arises because particles at small angles have to traverse more material before leaving the device in question.

For particles stopping in the inner tracker we would in principle also have to take into account the effects of the beam pipe. However since the thickness of the beam pipe is more than an order of magnitude smaller than that of the inner tracker, we have neglected the effects of the beam pipe when considering the stopping in the inner tracker.

3 Limits from Monojet and Monophoton searches

3.1 Monojet searches

As a first example let us now consider the limits from the CMS monojet search [6]. We focus on the 8 TeV results, as the recent 13 TeV analyses employ model specific assumptions [25–28], making a direct comparison less reliable. The size of the data set is also not important for the qualitative impact of monojets on the discussed scenarios; we will extrapolate the 8 TeV limits to the 13 TeV run 2 expectation as well as to the end of the high luminosity phase.

To obtain these limits we have simulated the monojet process (cf. Fig. 2) and accepted only those events that are stopped in the respective parts of the detector, either the beam pipe or the inner tracker. Effectively this corresponds to a Q and η -dependent cut on the energy of the produced particles. The explicit value of this cut can be obtained by solving Eq. (2.9) for the energy as a function of Q and η . We require that both highly charged particles are stopped sufficiently early.

As already discussed in the previous section we consider two options where the particles can be stopped in order to be “invisible” and the signal to be counted in the monojet search (or the monophoton search below). It is clear that particles stopped in the beam pipe will not leave any detectable trace in the detector*. The situation is not so clear in the inner tracker. However, as the particle is stopped before it reaches the calorimeter, it does not leave an observable cluster there that could be associated to the stopped track. In any case, the large misbalance in transverse momentum for these events will leave these events triggered. Therefore, those events can be understood from a monojet search [29]. To be on the safe side we will perform our analysis for both cases (stopping in the beam pipe and in the inner tracker, respectively) and will reserve the interesting question of how detectable, yet non-standard signatures can be used to tighten constraints on HIPs to future work.

Nevertheless, before proceeding let us note that at this point there is at least one clear avenue for an improved analysis based on the detailed information on the events: looking at the monojet signals (the jet allowing it to be triggered) it should be possible to do a search for extra tracks/energy deposition in the inner tracker caused by the stopping of the strongly interacting particle. This is a clearly different signature from the Standard Model background events and should allow for a significant reduction in the background.

Let us now try to obtain some first limits, through interpreting the analysis of [6] in the present context. CMS define signal regions from inclusive E_T^{miss} bins. The details of the analysis (which reports a model-independent limit at 8 TeV) can be inferred from [6], but we summarise the key selection criteria here for completeness.

The CMS analysis is based on clustering jets with the anti- k_T algorithm [30] with a resolution parameter $D = 0.5$. The leading jet in the event needs obey the following transverse momentum and rapidity requirements

$$p_{T,j_1} > 110 \text{ GeV}, |\eta_{j_1}| < 2.4, \quad (3.1)$$

*Except maybe some δ -radiation originating from the stopping process.

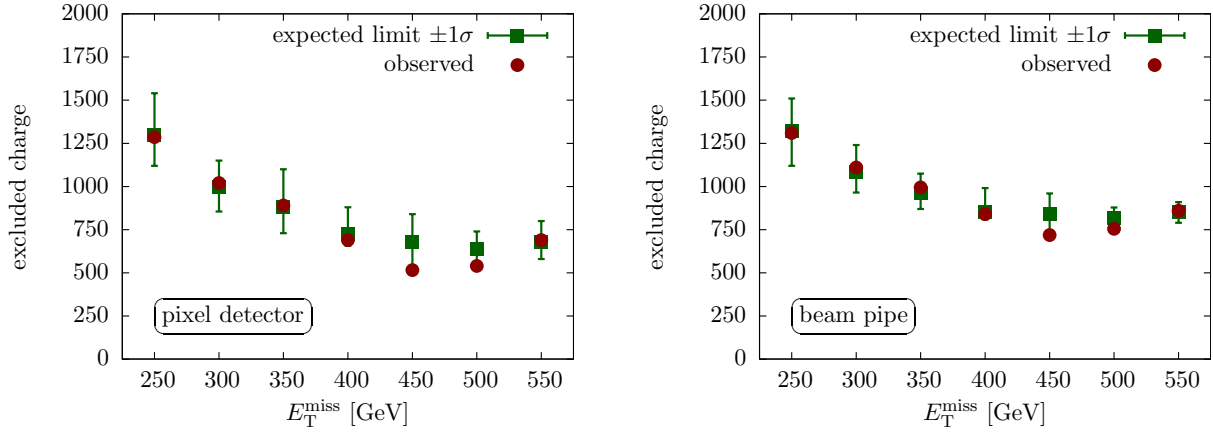


Figure 4: Limits on the maximal charge (in units of e) of a particle for the different E_T^{miss} bins considered in the CMS search [6]. Particles are required to be stuck in the inner tracker (left panel) or the beam pipe (right panel). For both examples we have chosen a particle mass of $m = 1000$ GeV.

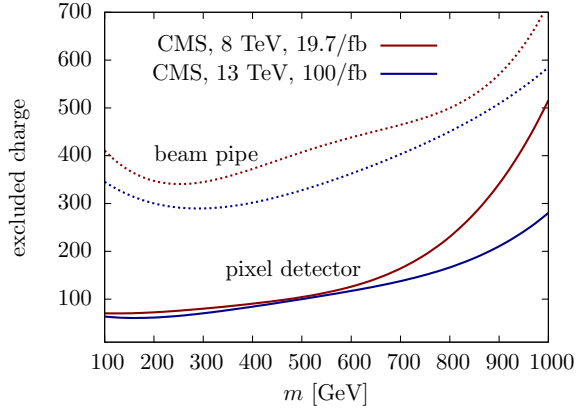


Figure 5: Limits on highly charged particles (in units of e) from the monojet search. The production process is assumed to be Drell-Yan plus jet. The dotted lines labelled “beam pipe” only take into account signal events where both produced highly charged particles are stopped in the beam pipe. The solid “pixel detector” lines require particles to be stopped in the inner tracker.

allowed charge of the particle for the setup described in Sec. 2.2. This demonstrates that the bins with higher E_T^{miss} are more sensitive for the case of a $m = 1$ TeV state as indicated in Fig. 2. The reason for this is that the high mass scale induced by the HIP leads to a signal that is clustered at relatively hard jet transverse momentum distribution $p_{T,j}$. Given that the contributing backgrounds are steeply falling distributions as a function of the $E_T^{\text{miss}} \sim p_{T,j}$, high E_T^{miss} selections provide the tightest constraints for large HIP masses.

Taking the bins from the CMS search into account and using the CLs method [31] to extrapolate the results of the 8 TeV analysis to 13 TeV, we obtain the limits shown in Fig. 5.

and an additional jet

$$p_{T,j_2} > 30 \text{ GeV}, |\eta_{j_2}| < 4.5 \quad (3.2)$$

is only allowed if it is consistent with a monojet signature

$$\Delta\Phi(j_1, j_2) < 2.5. \quad (3.3)$$

Events with more than two jets in the $p_T > 30$ GeV and $|\eta_j| < 4.5$ regions are vetoed as well as events with isolated leptons if $p_{T,\ell} > 10$ GeV. CMS define “isolation” by requiring that the total hadronic energy deposit in a cone of size $\Delta R \equiv \sqrt{\Delta\Phi^2 + \Delta\eta^2} < 0.4$ around the lepton candidate is smaller than 20% of the candidate’s p_T . The analysis focuses on seven inclusive search regions defined by the amount of observed missing energy.

In Fig. 4 we have considered each of these selections separately and rephrased the CMS constraints as a constraint on the maximal al-

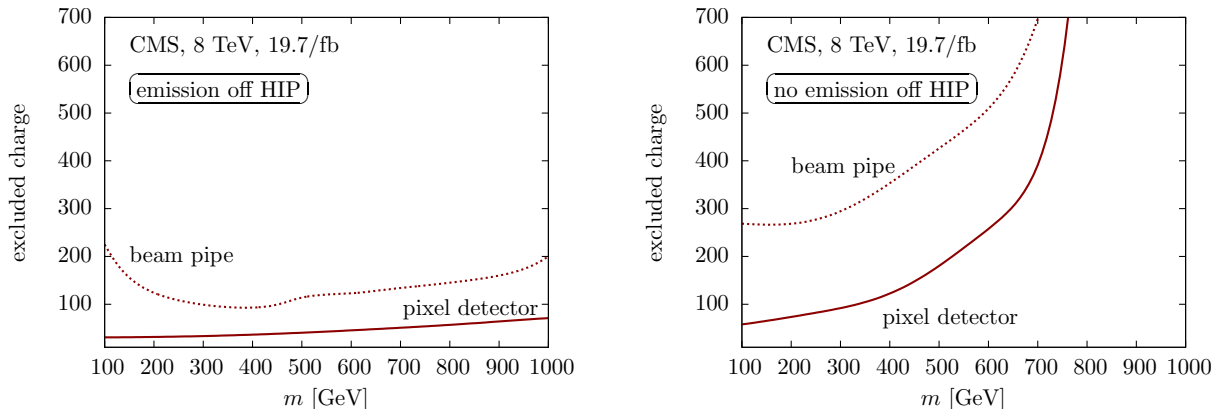


Figure 6: Limits on highly charged particles (in units of e) from the monophoton search [2]. As in Fig. 5 the dotted line only considers events stopped in the beam pipe, whereas the solid ones also allows for events stopped in the inner tracker the full monophoton signal, including both initial and final state radiation. In the right panel we only take into account initial state radiation.

3.2 Monophoton search

In analogy to the monojet search we can also use monophoton searches. As already mentioned in Sec. 2.1 there is one crucial difference to the monojet signal. The photon can also arise from final state radiation (cf. Fig. 3). In principle this could be advantageous because it significantly increases the signal. Indeed for large charges it results in a production cross section

$$\sigma(\text{monophoton}) \sim Q^4 \quad (3.4)$$

much larger than the[†]

$$\sigma(\text{monojet}) \sim Q^2. \quad (3.5)$$

For comparability we again choose to recast an analysis by CMS [2].

Again, anti- k_T jets with $D = 0.5$ are used and isolated photons are reconstructed through a similar isolation strategy as leptons: The energy deposit in a cone $\Delta R = \sqrt{\Delta\Phi^2 + \Delta\eta^2} < 0.3$ has to be smaller than 5% of the photon candidate's energy. At least one isolated photon with $E_T(\gamma) > 145$ GeV in $|\eta| \leq 1.44$. Events with more than a single jet with $p_T > 30$ GeV and light leptons (isolation is based on a hadronic energy deposit in the vicinity of $\Delta R < 0.3$ by less than 20% of the candidate's p_T) with $p_T > 10$ GeV are vetoed if they are well-separated from the photon by $\Delta R > 0.5$. In the last step the analysis focusses on a large missing transverse energy $E_T^{\text{miss}} > 140$ GeV, whose direction in the transverse plane needs to be well-separated (and back-to-back) to the photon $\Delta\Phi(E_T^{\text{miss}}, \gamma) > 2$.

The dependence of the production cross section on the charge for the different emission scenarios is reflected in the significantly better limits shown as the red lines in Fig. 6 (left panel) compared to the monojet analysis.

Similar conclusions directly generalise to mono- Z analyses, which, however are less sensitive compared to the monophoton case, and we therefore do not discuss them in detail.

However, as we will briefly discuss in the following section, we are in a deeply non-perturbative regime for highly charged particles. Therefore a simple perturbative treatment of the final state

[†]Of course this also indicates a breakdown of perturbation theory. We will briefly discuss this issue in the next section.

radiation (or perhaps even the production process itself) may be dubious. We therefore also show in Fig. 6 (right panel) the limits taking into account only initial state radiation such that the cross section is,

$$\sigma(\text{initial state radiation only, monophoton}) \sim Q^2. \quad (3.6)$$

4 Conceptual and technical issues with highly charged particles

As already indicated in the previous sections there are some problematic issues with highly charged particles. While we have ignored them in our general analysis, let us nevertheless briefly mention some of them in this section. In the next section we then discuss how the monophoton searches can be interpreted in a more general and perhaps slightly less model-dependent way.

Non-perturbativity

The first problem with highly charged particles is that we quickly enter a regime where QED is non-perturbative. The relevant expansion parameter is, an

$$\alpha Q^2 \sim 10^{-2} Q^2. \quad (4.1)$$

Even if we generously assume perturbativity up to $\alpha Q^2 \sim 4\pi$ we still have,

$$\alpha Q^2 \sim 4\pi, \quad \text{for } Q \sim 40, \quad (4.2)$$

severely limiting the range of perturbation theory.

Landau pole

Related to the question of non-perturbativity is that the Landau pole of QED will be very close to the *elementary* particle mass threshold and therefore within the region probed by the LHC.

For large charges we can neglect the contribution of the SM particles. The Landau pole is then at

$$\Lambda = m \exp\left(\frac{3\pi}{\alpha(m)Q^2}\right) \sim \exp(1) \quad \text{for } Q \gtrsim 35. \quad (4.3)$$

Again for sufficiently large charges $Q \gtrsim 35$ the Landau pole is less than a factor of e above the particle mass.

Schwinger pair production

The two problems discussed above affect the consistency of the theory. However, in principle there is also a practical consideration that may limit the stopping power of the high charges: at very high charges the field is self-shielding due to electron-positron pair production via the Schwinger mechanism [32]. Let us briefly also estimate this effect.

Schwinger pair production is a non-perturbative effect analog to tunneling. Its rate per volume is given by

$$\frac{d\Gamma}{dV} \sim m_e^4 \left(\frac{E}{E_c}\right)^2 \exp\left(-\frac{\pi E_c}{E}\right), \quad (4.4)$$

where E is the electrical field, m_e the electron mass and we have used the critical field for the production of electron-positron pairs,

$$E_c = \frac{m_e^2}{e}. \quad (4.5)$$

Pair production becomes fast when the critical field is exceeded in a volume larger than the Compton volume of the electron $V \sim 1/m_e^3$.

The electric field of a highly charged particle is,

$$E_Q \sim \frac{Qe}{4\pi r^2}. \quad (4.6)$$

If the field exceeds the critical field strength at a distance of two Compton length the condition for rapid pair production is certainly fulfilled in a volume of $\sim 8m_e^{-3}$. This is the case when

$$\frac{Qe^2}{16\pi} = \frac{\alpha Q}{4} \gtrsim 1 \quad \text{for} \quad Q \gtrsim 500. \quad (4.7)$$

Requiring rapid pair production only in a smaller volume $\sim m_e^{-3}$ the bound can be tightened by a factor of 4 to $Q \sim 100$. Comparing with the results from the previous section we see that self-shielding from pair production might be a significant effect.

5 Monojet and Monophoton searches for general stoppable particles

The objections discussed in the previous section are to a large degree specific to highly charged point-like particles. Non-elementary or extended objects such as magnetic monopoles may not suffer from all of these concerns.

Indeed our strategy to search for particles strongly interacting with the detector medium is more general. As long as the particle is produced from quarks it is likely that at least initial state radiation (gluons, photons or Z s) can be produced. Events where the produced new particles are stopped will then contribute to the monojet or monophoton signal.

In general it is difficult to determine model-independent limits. As discussed in Sect. 2 the fraction of events where the particle is stopped sufficiently early depends in general on the energy and angular distribution. Moreover, it will also depend on the energy dependence of the stopping process. That said, let us nevertheless take one step in the direction of a more general limit. Assuming that all these dependencies are the same as in the Drell-Yan + jet or Drell-Yan + photon process, we can at least allow for an arbitrary production cross section, e.g. the particles could additionally be produced from decays of other particles or there could be a form factor suppressing the production.

Other searches by ATLAS, CMS, LHCb, ALICE and MoEDAL are directly based on the Drell-Yan production cross section. To facilitate the comparison with our results we show in Fig. 7 our cross section limit expectations re-scaled to that of the Drell-Yan production without jets, i.e. we multiply by

$$\frac{\sigma(\text{Drell-Yan})}{\sigma(\text{Drell-Yan} + \text{jet})}. \quad (5.1)$$

This also allows for a comparison between the sensitivity of the monojet and monophoton searches in Fig. 7, where we also show extrapolations to 13 TeV data taking for the monojet

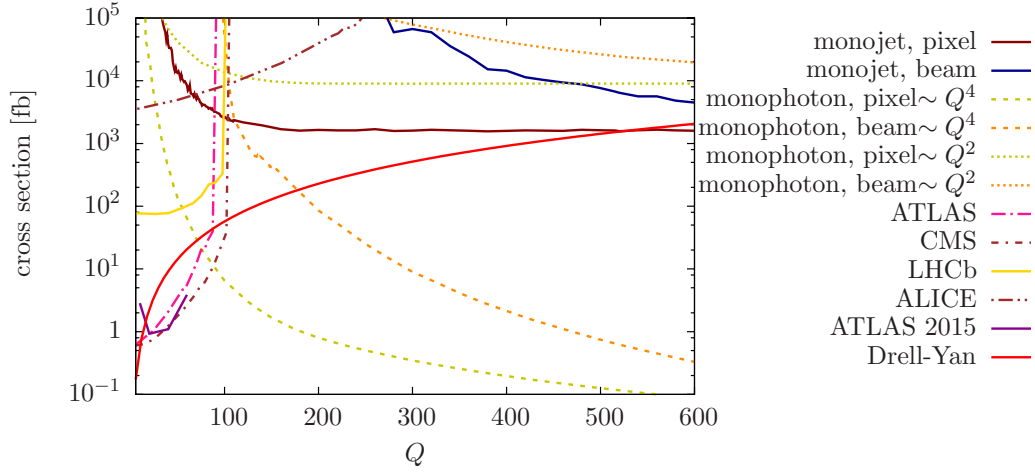


Figure 7: Limits on the production cross section from the monojet and monophoton searches as described in the text. For the angular and energy distributions we have assumed the same as for Drell-Yan + jet. Similarly we have assumed that the stopping has the same energy distribution as for a highly charged particle of mass 1000 GeV. We also include the projections by ATLAS, CMS, LHCb and ALICE according to Ref. [11] (which is obtained for 7 TeV collisions) as well as 2015 ATLAS constraint [20].

case, which is in general more sensitive when HIP emission is not included (and when the perturbative expansion is more reliable).

While the limits presented in this section are far from model-independent, they at least give an indication of the reach of the monojet and monophoton searches for particles that can be stopped in the material of the detector. While we expect details such as the angular distribution to be different, we also expect that in general particles with higher energy/momentum are less likely to be stopped. In consequence only those new particles that are produced with relatively

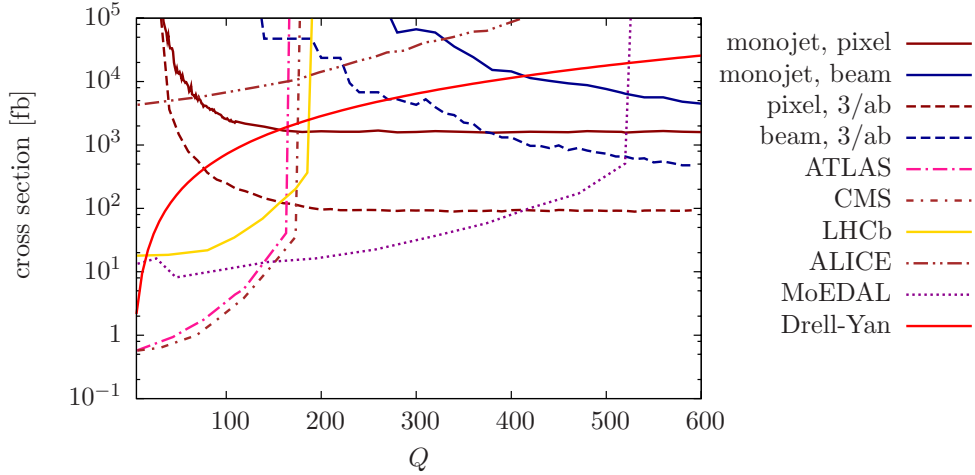


Figure 8: Same as Fig. 7 with 14 TeV projections from Ref. [11]. We also include monojet projections for the LHC high-luminosity run with 3000 fb^{-1} with conservative 13 TeV centre-of-mass energy, reducing the all systematics with the square root of the luminosity compared to Fig. 7.

small energy/momentum will contribute to the monojet/monophoton signal - a feature at least qualitatively represented by our Drell-Yan example.

6 Concluding Remarks

In this note we have argued that monojet and monophoton searches are powerful tools in searches for new particles that interact so strongly with the detector material that they are stopped before they reach parts of the detector which are essential for recording these events. If all of the new particles are stopped in the beam pipe there will be no signature in the actual detector[‡]. If there is additional initial and/or final state radiation the event will look like a monophoton or monojet final state. For the purposes of monojet and monophoton searches the same is likely to hold if the new particles are stopped in the tracker. The detector response to the new particles lacks the features (signals in the calorimeters or the muon detectors) that will allow the experiments to identify them as electrons, muons or jets. Consequently, the corresponding event is likely to be counted as part of a monosignature analysis. Yet, on closer inspection of the detector response such events will be very different from the SM background monojet/monophoton events, thereby opening the chance for significantly improved searches.

Here we have focussed our calculations on the concrete example of highly charged particles. The very high charges considered may raise questions about perturbativity, calculational methods and even the viability of the model (nevertheless we essentially use the same technical calculation of cross sections etc. as used in related searches[§]). Importantly, however, the general strategy proposed here should be more widely applicable, in particular also to the case of magnetic monopoles. The example of highly charged particles constrained by the recent CMS searches for monojets and monophotons demonstrates that our proposed search strategy has significant power complementary to existing search strategies at ATLAS, CMS, LHCb, ALICE as well as dedicated detectors such as MoEDAL.

Acknowledgements

We thank Hans-Christian Schultz-Coulon and Shahram Rahatlou for helpful discussions. We also thank the organisers of the 2016 Patras Workshop for providing the environment where this work was initiated. J.J. gratefully acknowledges support by the DFG TR33 “The Dark Universe” as well as the European Unions Horizon 2020 research and innovation programme under the Marie Skłodowska-Curie grant agreement Numbers 674896 and 690575.

References

- [1] **ATLAS** Collaboration, G. Aad *et. al.*, *Search for new phenomena in events with a photon and missing transverse momentum in pp collisions at $\sqrt{s} = 8$ TeV with the ATLAS detector*, *Phys.Rev.* **D91** (2015), no. 1 012008, [[arXiv:1411.1559](#)].

[‡]Except maybe from cascades caused by the stopping process, e.g. δ -electrons.

[§]However, pointing out one caveat is in order. The potential shielding caused by Schwinger pair production would probably increase the signal in searches looking for highly ionizing tracks, while decreasing the monosignatures. However, this is largely specific to the case of highly charged particles.

- [2] **CMS** Collaboration, V. Khachatryan *et. al.*, *Search for new phenomena in monophoton final states in proton-proton collisions at $\sqrt{s} = 8$ TeV*, [arXiv:1410.8812](#).
- [3] **ATLAS** Collaboration, G. Aad *et. al.*, *Search for dark matter in events with a Z boson and missing transverse momentum in pp collisions at $\sqrt{s}=8$ TeV with the ATLAS detector*, *Phys.Rev.* **D90** (2014), no. 1 012004, [[arXiv:1404.0051](#)].
- [4] **CMS** Collaboration, V. Khachatryan *et. al.*, *Search for physics beyond the standard model in final states with a lepton and missing transverse energy in proton-proton collisions at $\sqrt{s} = 8$ TeV*, [arXiv:1408.2745](#).
- [5] **ATLAS** Collaboration, G. Aad *et. al.*, *Search for dark matter in events with a Z boson and missing transverse momentum in pp collisions at $\sqrt{s}=8$ TeV with the ATLAS detector*, *Phys.Rev.* **D90** (2014), no. 1 012004, [[arXiv:1404.0051](#)].
- [6] **CMS** Collaboration, V. Khachatryan *et. al.*, *Search for dark matter, extra dimensions, and unparticles in monojet events in proton-proton collisions at $\sqrt{s} = 8$ TeV*, [arXiv:1408.3583](#).
- [7] P. A. M. Dirac, *Quantized Singularities in the Electromagnetic Field*, *Proc. Roy. Soc. Lond.* **A133** (1931) 60–72.
- [8] P. A. M. Dirac, *The Theory of magnetic poles*, *Phys. Rev.* **74** (1948) 817–830.
- [9] **MoEDAL** Collaboration, J. Pinfold *et. al.*, *Technical Design Report of the MoEDAL Experiment*, 2009.
- [10] **MoEDAL** Collaboration, B. Acharya *et. al.*, *Search for magnetic monopoles with the MoEDAL prototype trapping detector in 8 TeV proton-proton collisions at the LHC*, *JHEP* **08** (2016) 067, [[arXiv:1604.0664](#)].
- [11] A. De Roeck, A. Katre, P. Mermod, D. Milstead, and T. Sloan, *Sensitivity of LHC Experiments to Exotic Highly Ionising Particles*, *Eur. Phys. J.* **C72** (2012) 1985, [[arXiv:1112.2999](#)].
- [12] **CMS** Collaboration, S. Chatrchyan *et. al.*, *Searches for long-lived charged particles in pp collisions at $\sqrt{s}=7$ and 8 TeV*, *JHEP* **07** (2013) 122, [[arXiv:1305.0491](#)].
- [13] **ATLAS** Collaboration, G. Aad *et. al.*, *Search for long-lived stopped R-hadrons decaying out-of-time with pp collisions using the ATLAS detector*, *Phys. Rev.* **D88** (2013), no. 11 112003, [[arXiv:1310.6584](#)].
- [14] **CMS** Collaboration, V. Khachatryan *et. al.*, *Search for Displaced Supersymmetry in events with an electron and a muon with large impact parameters*, *Phys. Rev. Lett.* **114** (2015), no. 6 061801, [[arXiv:1409.4789](#)].
- [15] **ATLAS** Collaboration, G. Aad *et. al.*, *Search for nonpointing and delayed photons in the diphoton and missing transverse momentum final state in 8 TeV pp collisions at the LHC using the ATLAS detector*, *Phys. Rev.* **D90** (2014), no. 11 112005, [[arXiv:1409.5542](#)].

- [16] **ATLAS** Collaboration, G. Aad *et. al.*, *Searches for heavy long-lived charged particles with the ATLAS detector in proton-proton collisions at $\sqrt{s} = 8$ TeV*, *JHEP* **01** (2015) 068, [[arXiv:1411.6795](#)].
- [17] **CMS** Collaboration, V. Khachatryan *et. al.*, *Search for Decays of Stopped Long-Lived Particles Produced in Proton-Proton Collisions at $\sqrt{s} = 8$ TeV*, *Eur. Phys. J.* **C75** (2015), no. 4 151, [[arXiv:1501.0560](#)].
- [18] **ATLAS** Collaboration, G. Aad *et. al.*, *Search for heavy long-lived multi-charged particles in pp collisions at $\sqrt{s} = 8$ TeV using the ATLAS detector*, *Eur. Phys. J.* **C75** (2015) 362, [[arXiv:1504.0418](#)].
- [19] **ATLAS** Collaboration, G. Aad *et. al.*, *Search for massive, long-lived particles using multitrack displaced vertices or displaced lepton pairs in pp collisions at $\sqrt{s} = 8$ TeV with the ATLAS detector*, *Phys. Rev.* **D92** (2015), no. 7 072004, [[arXiv:1504.0516](#)].
- [20] **ATLAS** Collaboration, G. Aad *et. al.*, *Search for magnetic monopoles and stable particles with high electric charges in 8 TeV pp collisions with the ATLAS detector*, *Phys. Rev.* **D93** (2016), no. 5 052009, [[arXiv:1509.0805](#)].
- [21] **CMS** Collaboration, C. Collaboration, *Searches for Long-lived Charged Particles in Proton-Proton Collisions at $\sqrt{s} = 13$ TeV*, .
- [22] **ATLAS** Collaboration, M. Aaboud *et. al.*, *Search for metastable heavy charged particles with large ionization energy loss in pp collisions at $\sqrt{s} = 13$ TeV using the ATLAS experiment*, *Phys. Rev.* **D93** (2016), no. 11 112015, [[arXiv:1604.0452](#)].
- [23] **ATLAS** Collaboration, M. Aaboud *et. al.*, *Search for heavy long-lived charged R-hadrons with the ATLAS detector in 3.2 fb^{-1} of proton-proton collision data at $\sqrt{s} = 13$ TeV*, *Phys. Lett.* **B760** (2016) 647–665, [[arXiv:1606.0512](#)].
- [24] **Particle Data Group** Collaboration, K. A. Olive *et. al.*, *Review of Particle Physics*, *Chin. Phys.* **C38** (2014) 090001.
- [25] **CMS Collaboration** Collaboration, *Search for dark matter and unparticles in events with a Z boson and missing transverse momentum in proton-proton collisions at $\sqrt{s} = 13$ TeV*, Tech. Rep. CMS-PAS-EXO-16-010, CERN, Geneva, 2016.
- [26] **CMS Collaboration** Collaboration, *Search for dark matter in $Z + E_{\text{T}}^{\text{miss}}$ events using 12.9 fb^{-1} of 2016 data*, Tech. Rep. CMS-PAS-EXO-16-038, CERN, Geneva, 2016.
- [27] **CMS Collaboration** Collaboration, *Search for dark matter and graviton produced in association with a photon in pp collisions at $\sqrt{s} = 13$ TeV with an integrated luminosity of 12.9 fb^{-1}* , Tech. Rep. CMS-PAS-EXO-16-039, CERN, Geneva, 2016.
- [28] **CMS Collaboration** Collaboration, *Search for dark matter in final states with an energetic jet, or a hadronically decaying W or Z boson using 12.9 fb^{-1} of data at $\sqrt{s} = 13$ TeV*, Tech. Rep. CMS-PAS-EXO-16-037, CERN, Geneva, 2016.
- [29] H.-C. Schultz-Coulon and S. Rahatlou, *personal communication*, 2016.

- [30] M. Cacciari, G. P. Salam, and G. Soyez, *The Anti- $k(t)$ jet clustering algorithm*, *JHEP* **04** (2008) 063, [[arXiv:0802.1189](#)].
- [31] A. L. Read, *Presentation of search results: The $CL(s)$ technique*, *J. Phys.* **G28** (2002) 2693–2704. [[11\(2002\)](#)].
- [32] J. S. Schwinger, *On gauge invariance and vacuum polarization*, *Phys. Rev.* **82** (1951) 664–679.